Ag growth on the Ag$_2$Bi Rashba alloy

Sanjoy Kr Mahatha[1,2], Polina M. Sheverdyaeva[2], Carlo Carbone[2], and Paolo Moras[2]

[1]*School of Physics and Materials Science, Thapar Institute of Engineering and Technology, Patiala - 147004, India.*

[2]*Istituto di Struttura della Materia-CNR (ISM-CNR), SS 14 km 163.5, I-34149 Trieste, Italy*

Multilayer structures comprising Bi/Ag bilayers display spin-charge conversion, a phenomenon of interest in spintronics whose origin (inverse Rashba-Edelstein vs. inverse spin Hall effects) is still debated. The Bi/Ag interfaces are assumed to be stable in model calculations, but the experimental determination of their structural properties is missing. Here, we explore by photoemission spectroscopy the stability and electronic structure of a Bi/Ag interface with strong Rashba interaction. We saturate the surface of a Ag(111) crystal with the Ag$_2$Bi alloy, which presents surface-embedded Bi atoms and characteristic Rashba-split surface states, and deposit Ag layers on top of it at room temperature. The intensity of the Rashba-split bands weakens sizably after the deposition of few Ag monolayers, although most of the Bi atoms segregate at the surface and retain the original local coordination. These findings are consistent with the surfactant behavior of Bi atoms, which favors a layer-by-layer Ag growth without preserving the long range order of the Ag$_2$Bi alloy. They also suggest the need of detailed chemical and structural analysis for an accurate description of Bi/Ag bilayers.

I. INTRODUCTION

The Rashba effect arises from the spin-orbit coupling and the breaking of the discrete translational symmetry occurring at the surface of a crystal or at the interface between crystals [1]. An effective magnetic field lifts the spin-degeneracy of the electronic structure: the bands are offset towards opposite directions in the parallel momentum ($k_{\parallel}$) plane according to their spin [2-4]. The effect is particularly strong ("giant") in the substitutional Ag_2Bi surface alloy on Ag(111) [5-8] due to the large spin-orbit coupling of Bi and the out-of-plane structural modulation of the alloy [9-12].

The experimental observation of the giant Rashba effect suggested its exploitation for spintronic applications. Spin-pumping measurements show that a spin current injected from a ferromagnetic NiFe layer into a Bi/Ag bilayer is converted efficiently into an electron current by the inverse Rashba-Edelstein effect, as the Rashba spin-orbit interaction is assumed to be strong at the Bi/Ag interface [13]. Alternative interpretations are based on the inverse spin-Hall effect [14,15]. Notably, the spin-charge conversion is also observed when the Ag layer is terminated by the Ag_2Bi surface alloy [14]. These results call for a deeper analysis of the Bi/Ag interfaces, with focus on the formation and role of the Ag-Bi alloys.

In the present study we examine by photoelectron spectroscopy the electronic and structural properties of nanometer thick Ag layers deposited at room temperature on the Ag_2Bi surface alloy on Ag(111). Core level analysis shows that most of the Bi atoms segregate to the surface, irrespectively of the amount of deposited Ag, and retain the embedded atomic coordination of the alloy. Instead, the ARPES signal of the Rashba-split bands, which monitors the long range order of the Ag_2Bi domains, worsens quickly as a function of the Ag thickness. These observations are ascribed to the surfactant behavior of Bi, in close analogy to the case of Sb on Ag(111) [16]: the surface embedded Bi atoms drive the layer-by-layer growth of Ag, while the buried Ag_2Bi alloy is unstable with respect to the deposition of Ag. We suggest that strong spin-orbit effects in Bi/Ag bilayers displaying efficient spin-charge conversion could be associated to the presence of Bi atoms embedded in the Ag layers.

II. METHODS

The experiment was performed at the VUV-Photoemission beamline of the synchrotron Elettra (Trieste, Italy). This laboratory is equipped with a Scienta R4000 electron spectrometer. The angle between the photon beam (horizontal polarization) and the analyzer is 45°. The photoelectrons are collected within the light scattering plane. The energy and angular resolutions were set to 30 meV and 0.3°. The Ag(111) single crystal surface was prepared by sputtering and annealing cycles until a

sharp low-energy electron diffraction (LEED) pattern and an intense Shockley surface state was observed near $k_\parallel = 0$ by ARPES (left panel of Fig. 1). After Bi deposition the sample was annealed to 360 K to favor the formation of a well ordered Ag_2Bi alloy displaying the characteristic $(\sqrt{3}\times\sqrt{3})R30°$ LEED pattern [5]. The optimal Bi coverage to saturate the whole surface with the Ag_2Bi alloy (1/3 of a monolayer on the Ag(111) surface, 1 Ag ML = 2.36 Å) was found in correspondence with the maximal intensity of the "$\sqrt{3}$" LEED spots and of the Rashba-split surface states (right panel of Fig. 1). Ag was deposited on the Ag_2Bi alloy at room temperature. After each Ag deposition the system was annealed to 360 K. All the photoemission data were taken at room temperature and in normal emission geometry. Angle-resolved and angle-integrated photoemission spectra were measured using 40 and 70 eV photon energies, respectively.

III. RESULTS AND DISCUSSION

In the substitutional Ag_2Bi surface alloy on Ag(111) every third Ag atom along the Ag[110] direction is replaced by a Bi atom (Ag-embedded coordination). Due to their large atomic radius, Bi atoms present an upward shift of 0.65 Å with respect to the topmost Ag layer [17]. This experimental value was found to be in between the theoretical values of 0.35 Å [18] and 0.85 Å [9] obtained using different structural relaxation methods. The combination of the large atomic spin-orbit coupling of Bi and the outward relaxation gives rise to a giant spin-splitting of the $6sp_z$- and $6p_xp_y$-derived surface bands. The right panel of Fig. 1 shows ARPES data for the Ag_2Bi alloy on Ag(111) at optimal preparation conditions. The $6sp_z$-derived states are identified with the downward dispersive bands which are shifted sideways with respect to $k_\parallel = 0$ by the giant Rashba effect, in agreement with Ref. [5]. Under the experimental conditions used in the present experiment the $6p_xp_y$-derived bands are barely visible.

The Ag_2Bi surface alloy on Ag(111) is taken as the starting point for a sequence of Ag depositions and annealing. The angle-integrated spectra labelled from 1 to 6 in Fig. 2(a) are used to monitor the electronic structure and the chemical composition of the surface layers at different stages. The spectra cover the region from the Bi$5d$ core levels (orange shaded area) up to the Fermi level. The blue shaded area highlights the Ag$4d$ levels, which are the dominant features near the Fermi level, while the emission from the Bi$6sp$ valence states is comparatively negligible. This is due to the different photoemission cross sections of the Ag$4d$ and Bi$6sp$ levels (36 times higher for Ag at 70 eV photon energy [19]) and the stoichiometry of the system (bulk Ag vs. 1/3 Bi ML). The bottommost spectrum gives the reference intensities for the Bi$5d$ and the Ag$4d$ levels at optimal alloy growth parameters. The other spectra correspond to alternate depositions of Ag layers (thickness in ML) and annealing

to 360 K. Despite the deposition of Ag layers all spectra are very similar. Small changes of the Ag4d lineshape are attributed to slight differences in the alignment of the sample in front of the electron analyzer of less than 1°. The Bi5d peaks have identical binding energy (23.60 eV for Bi5$d_{5/2}$ and 26.65 eV for Bi5$d_{3/2}$) and lineshape along the whole sequence of spectra. As an example, Fig. 2(b) shows a zoom of the Bi5d levels of the optimal Ag$_2$Bi surface alloy and at the preparation stage 5. These observations demonstrate that the local coordination and chemical environment of the Bi atoms closely resemble those of Bi in the Ag$_2$Bi surface alloy.

Fig. 2(c) shows with full circles the ratio between the areas of the Bi5d and Ag4d peaks (I_{Bi}/I_{Ag}, error bar ±5%). This ratio presents a small decrease with respect to the reference value of 0.365 (dashed line) along the sequence of Ag depositions and annealing. The decrease caused by the Ag depositions is not compatible with a Ag$_2$Bi alloy buried below uniform Ag layers, as shown in the following. We calculated the expected areal I_{Bi}/I_{Ag} ratios for the different Ag depositions (open circles in Fig. 2(c)). The systems are modeled as slabs of 13 atomic layers, with the Ag$_2$Bi alloy layer at various depths from the surface (2 ML below the surface at stage 2, etc.) and 12 Ag ML filling the remaining space. The thickness of Ag$_2$Bi alloy layer is assumed to correspond to that of 1 Ag ML. The inelastic mean free path for Bi5d and Ag4d photoelectrons (40 and 60 eV kinetic energy at 70 eV photon energy, respectively) is taken to be equal to $\lambda = 2$ Ag ML (4.72 Å). This short λ justifies the truncation of the systems to 13 atomic layers, as the photoelectron signal from deeper layers is negligible. I_{Bi} can be easily determined as:

$$I_{Bi} = I_{Bi,0}\, e^{-d/\lambda} \qquad (1)$$

where $I_{Bi,0}$ is the experimental area of the Bi5d peaks for the reference system and d the thickness of the deposited Ag layer (in ML). The determination of I_{Ag} is slightly more complex. Let's define I_{ML} as the area of the Ag4d photoemission peaks of 1 Ag ML. Then, I_{Ag} can be expressed as:

$$I_{Ag} = I_{ML} \sum_{n=1}^{13} a_n e^{-(n-1)/2} \qquad (2)$$

where n indexes the atomic layer (n = 1 is the surface layer) and a_n is the fraction of Ag atoms in the layer. Basically, $a_n = 0.66$ for the Ag$_2$Bi alloy and $a_n = 1$ for all other atomic layers. For the Ag$_2$Bi-terminated system Eq. 2 gives $I_{Ag,0} = 2.198\, I_{ML}$, where $I_{Ag,0}$ is the experimental reference value. This allows to write:

$$I_{Ag} = \frac{I_{Ag,0}}{2.198} \sum_{n=1}^{13} a_n e^{-(n-1)/2} \qquad (3)$$

Table 1 and Fig. 2(c) compare the I_{Bi}/I_{Ag} ratio derived from the model to the experimental I_{Bi}/I_{Ag} ratio for different Ag thickness. The discrepancy of the two datasets is evident. The experimental ratio $I_{Bi}/I_{Bi,0}$ (rightmost column of Table 1) suggests that most of the Bi atoms migrate towards the surface after the Ag depositions. A minor fraction of Bi atoms, which is evaluated to be few percent of the original Bi quantity, remains buried inside the deposited Ag layers or close to the original position. Post-deposition annealing promotes the surface segregation of a part of these Bi atoms and explains the small oscillations of the experimental I_{Bi}/I_{Ag} ratio observed in Fig 2(c).

d (in ML)	I_{Bi}/I_{Ag} (model)	I_{Bi}/I_{Ag} (exp.)	$I_{Bi}/I_{Bi,0}$ (%)
2	0.122	0.342	93.7
6	0.016	0.339	92.9
12	0.001	0.326	89.3

TAB. 1. Comparison of the I_{Bi}/I_{Ag} ratios derived from the model and the experiment and experimental $I_{Bi}/I_{Bi,0}$ ratio for the different Ag depositions.

Further insights into the system are obtained by the ARPES spectra of Fig. 3. The Ag deposition causes a worsening of the ARPES signal from the Rashba-split bands (stages 1, 3, 5), which is only partially restored after annealing to 360 K (stages 2, 4, 6). The central column of Fig. 3 shows that for the thickest Ag layer the Rashba-split bands are difficult to identify even after applying the first derivative procedure (along the energy axis), which enhances the contrast of weak spectral features. This trend can be described through A_R and A_B that represent the integral of the photoemission signal near the crossing point of the Rashba-split bands and away from Bi-derived bands (background). The areas of integration are displayed explicitly by two boxes in the right panel of Fig. 1 (reference spectrum) and in panels (1-6) of Fig. 3. The normalized signal from the Rashba-split bands ((A_R-A_B)/A_B, error bar $\pm 5\%$) is reported in Fig. 2(c) to allow a direct comparison with the core level signal. The Bi-related ARPES signal decreases much more pronouncedly than the corresponding signal of the Bi$5d$ levels as a function of the Ag thickness.

The spectroscopic observations reported above can be interpreted in different ways. The worsening of the ARPES signal could be ascribed to the co-existence of different Bi atom environments, as for instance Bi clusters. However, in this case we would observe a shift of the Bi core levels towards higher binding energies, as suggested by the position of the Bi5d peaks of a thick

(bulk-like) Bi layer (topmost spectrum in Fig. 2(b)). Instead, the close correspondence of the Bi core levels at all stages of Ag deposition and annealing suggests that the Bi atoms keep the atomic coordination they have in the Ag_2Bi alloy, i.e. they remain embedded on the Ag surface and surrounded by 6 Ag atoms. This scenario was experimentally demonstrated by scanning tunneling microscopy for up to 1 ML Ag depositions on $Ag_2Bi/Ag(111)$, where the ordered Ag_2Bi alloy persists on the surface [20]. As for the deposition of thicker Ag layers, our observations can be described consistently as due to the surfactant behavior of Bi, in close analogy with the well-documented case of Sb-guided growth of Ag on Ag(111) [16,21]. The presence of Sb turns the three-dimensional homo-epitaxial growth of Ag into a layer-by-layer growth. This growth mode is observed over a wide range of Sb concentrations (0.08-0.3 ML) and mediated by the presence of surface embedded Sb atoms, which lower the Ag mobility, favor the step-down mass transport of Ag ad-atoms and migrate easily to the Ag surface [16]. The process does not preserve the $(\sqrt{3}\times\sqrt{3})R30°$ order of the Ag_2Sb surface alloy, as the Sb atoms tend to accumulate on the step edges of the growing Ag layers [16]. These properties can explain likewise the different trends of the Bi$5d$ and ARPES signal (Fig. 2(c)): most of the Bi atoms reach the surface and display the embedded local coordination, but the initial long-range order of the Ag_2Bi alloy fades as a function of the Ag thickness. Annealing improves the surface order by the aggregation of Bi atoms to form larger Ag_2Bi domains, thus increasing the intensity of the Rashba-split bands.

IV. CONCLUSIONS

Our spectroscopic data shed light onto the growth of Ag layers on the $Ag_2Bi/Ag(111)$ surface. Ag grows in a layer-by-layer mode thanks to the surfactant behavior of the surface-embedded Bi atoms. No specific effect is attributed to the presence of the ordered Ag_2Bi alloy, which is unstable with respect to the deposition of Ag. Our results give a hint for the interpretation of the spin-pumping measurements that revealed the spin-charge conversion in multilayer structures containing Bi/Ag bilayers. These devices were synthesized by sequential depositions of Bi, Ag and NiFe films on a semiconductor substrate at room temperature. Under these growth conditions the Bi/Ag interfaces appear to be unstable. We suggest that strong spin-orbit coupling effects could be associated to the presence of Bi atoms embedded in the Ag layer. Further structural and chemical analysis of the buried Bi/Ag interfaces, for instance by high-energy photoemission spectroscopy, is needed to explore this scenario.

REFERENCES

[1] Y. A. Bychkov and E. I. Rashba JETP Lett. **39**, 78 (1984).

[2] S. LaShell, B. A. McDougall, and E. Jensen, Phys. Rev. Lett. **77**, 3419 (1996).

[3] Y. M. Koroteev, G. Bihlmayer, J. E. Gayone, E. V. Chulkov, S. Blügel, P. M. Echenique, and P. Hofmann, Phys. Rev. Lett. **93**, 046403 (2004).

[4] K. Yaji, A. Harasawa, K. Kuroda, R. Li, B. Yan, F. Komori, and S. Shin, Phys. Rev. B **98**, 041404(R) (2018).

[5] C. R. Ast, J. Henk, A. Ernst, L. Moreschini, M. C. Falub, D. Pacilé, P. Bruno, K. Kern, and M. Grioni, Phys. Rev. Lett. **98**, 186807 (2007).

[6] K. He, Y. Takeichi, M. Ogawa, T. Okuda, P. Moras, D. Topwal, A. Harasawa, T. Hirahara, C. Carbone, A. Kakizaki, and I. Matsuda, Phys. Rev. Lett. **104**, 156805 (2010).

[7] G. Bian, L. Zhang, Y. Liu, T. Miller, and T.-C. Chiang, Phys. Rev. Lett. **108**, 186403 (2012).

[8] C. Carbone, P. Moras, P. M. Sheverdyaeva, D. Pacilé, M. Papagno, L. Ferrari, D. Topwal, E. Vescovo, G. Bihlmayer, F. Freimuth, Y. Mokrousov, and S. Blügel, Phys. Rev. B **93**, 125409 (2016).

[9] G. Bihlmayer, S. Blügel, E.V. Chulkov, Phys. Rev. B **75** 195414 (2007).

[10] J. Premper, M. Trautmann, J. Henk, and P. Bruno, Phys. Rev. B **76**, 073310 (2007).

[11] S. Mathias, A. Ruffing, F. Deicke, M. Wiesenmayer, I. Sakar, G. Bihlmayer, E. V. Chulkov, Yu. M. Koroteev, P. M. Echenique, M. Bauer, and M. Aeschlimann, Phys. Rev. Lett. **104**, 066802 (2010).

[12] H. Bentmann, T. Kuzumaki, G. Bihlmayer, S. Blügel, E. V. Chulkov, F. Reinert, and K. Sakamoto, Phys. Rev. B **84**, 115426 (2011).

[13] J.C. Rojas Sánchez, L. Vila, G. Desfonds, S. Gambarelli, J.P. Attané, J.M. De Teresa, C. Magén, and A. Fert, Nat. Cummun. **4**, 2944 (2013).

[14] J. Li, P. Xu, J. Shen, Y. Cai, and X. Jin, J. Magn. Magn. Mater. **540**, 168471 (2021).

[15] J. Shen, Z. Feng, P. Xu, D. Hou, Y. Gao, and X. Jin, Phys. Rev. Lett. **126**, 197201 (2021).

[16] J. Vrijmoeth, H. A. van der Vegt, J. A. Meyer, E. Vlieg, and R. J. Behm, Phys. Rev. Lett. **72**, 3843 (1994).

[17] I. Gierz, B. Stadtmüller, J. Vuorinen, M. Lindroos, F. Meier, J. H. Dil, K. Kern, and C. R. Ast, Phys. Rev. B **81**, 245430 (2010).

[18] C. R. Ast, G. Wittich, P. Wahl, R. Vogelgesang, D. Pacilé, M. C. Falub, L. Moreschini, M. Papagno, M. Grioni, and K. Kern, Phys. Rev. B **75**, 201401(R) (2007).

[19] J.J. Yeh and I. Lindau, At. Data Nucl. Data Tables, **32**, 1-155 (1985).

[20] H. Fukumoto, M. Miyazaki, Y. Aoki, K. Nakatsuji, and H. Hirayama, Surface Science **611**, 49 (2013).

[21] H. A. van der Vegt, H. M. van Pinxteren, M. Lohmeier, E. Vlieg, and J. M. C. Thornton, Phys. Rev. Lett. **68**, 3335 (1992).
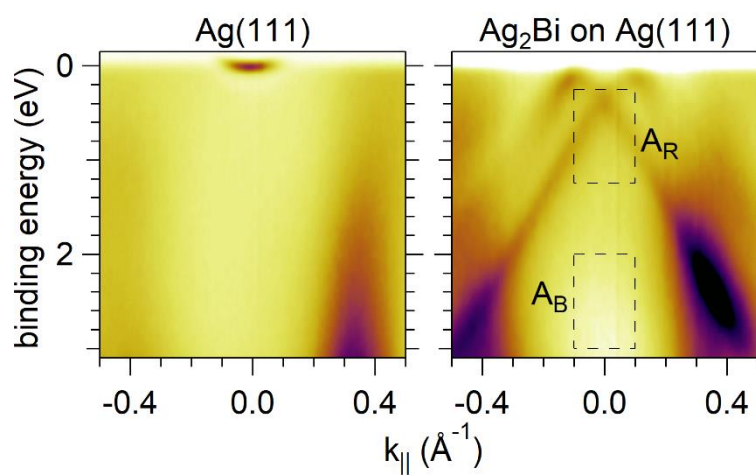
FIGURE 1: ARPES data for clean Ag(111) and Ag$_2$Bi/Ag(111) surfaces. The two boxes indicate the regions of integration of the ARPES signal to obtain A$_R$ and A$_B$.
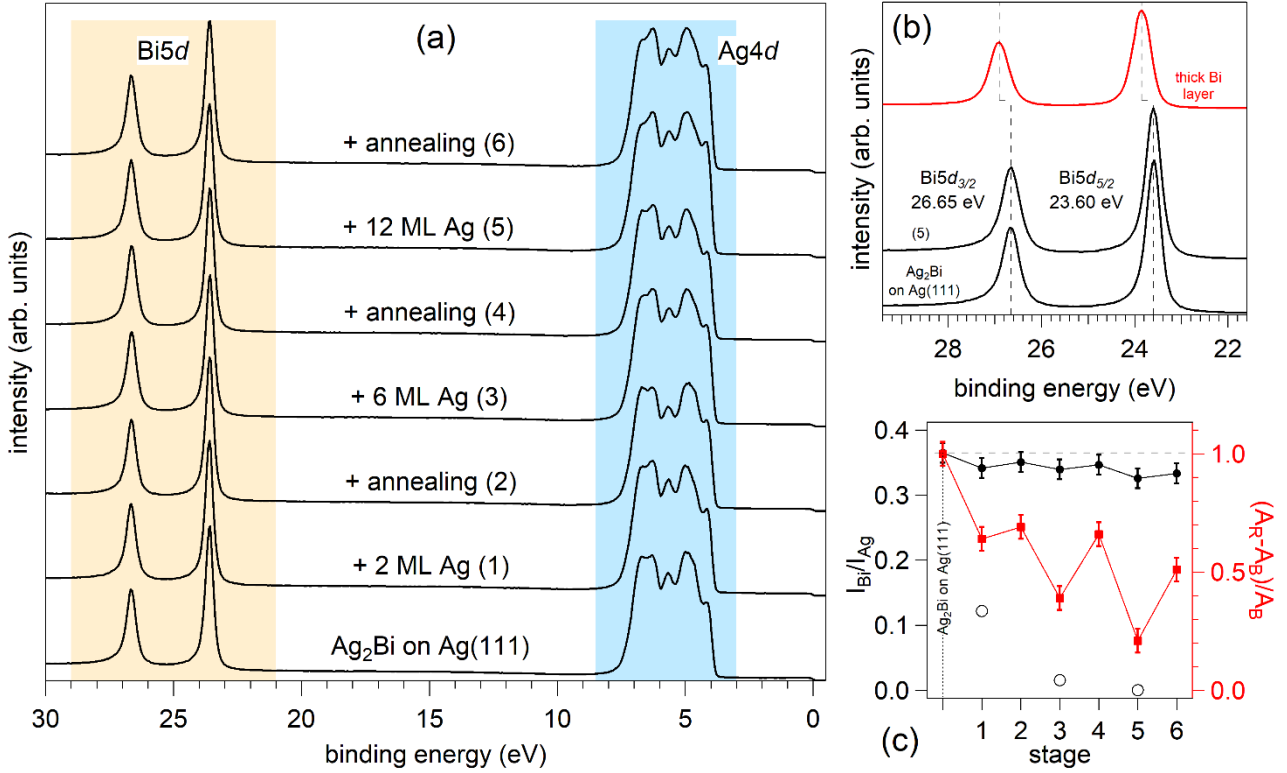
FIGURE 2: (a) Angle-integrated photoemission spectra for the reference $Ag_2Bi/Ag(111)$ system and for various stages of preparation (labeled 1 to 6). The orange and blue shaded areas indicate the energy ranges for the evaluation of I_{Bi} and I_{Ag}. (b) Zoom of the Bi5d levels for the original $Ag_2Bi/Ag(111)$ system and for stage 5. The topmost spectrum refers to a thick (bulk-like) Bi layer grown on Ge(111). The Bi5d levels present a downwards shift of 0.25 eV with respect to the spectra below. (c) Comparison between the experimental I_{Bi}/I_{Ag} ratio (full circles) and the expected I_{Bi}/I_{Ag} ratio if a uniform Ag layer grows on top of the Ag_2Bi alloy (open circles). The dashed line represents the ratio for the original $Ag_2Bi/Ag(111)$ system. Full squares display the normalized ratio of the ARPES signal of the Rashba-split bands (right vertical axis).
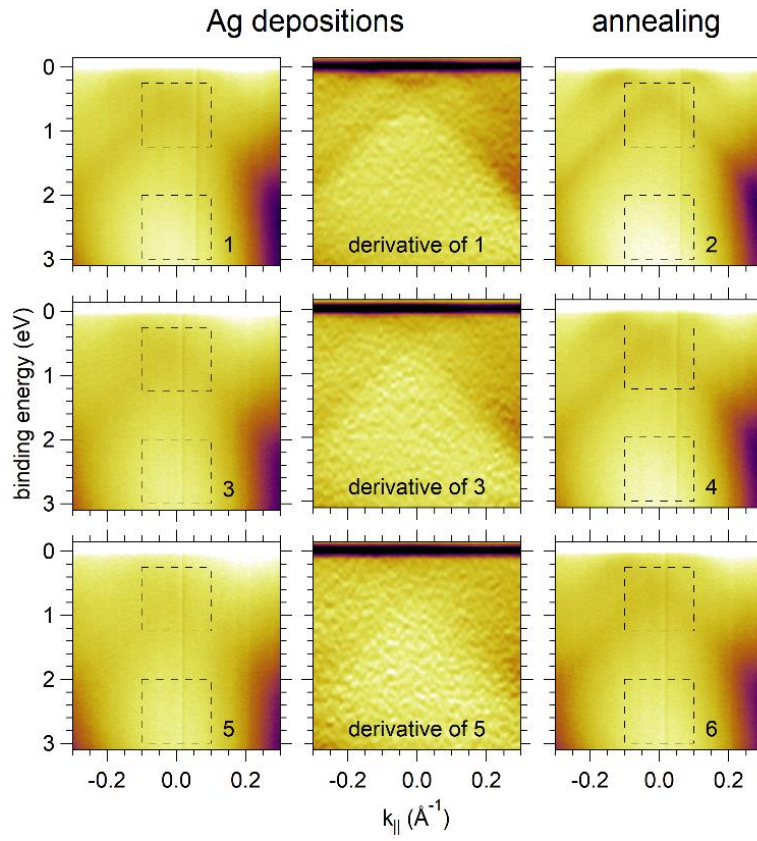
FIGURE 3: ARPES data for the Ag depositions (stages 1, 3, 5) and annealing (stages 2, 4, 6). The first derivative of the data for the Ag depositions (central column) are taken along the energy axis. The boxes indicate the regions of integration of the ARPES signal to obtain A_R and A_B.